Available online at www.sciencedirect.com
ScienceDirect
International Journal of Solids and Structures 45 (2008) 3410–3429
INTERNATIONAL JOURNAL OF SOLIDS AND STRUCTURES
www.elsevier.com/locate/ijsolstr

Asymmetric bifurcations of thick-walled circular cylindrical elastic tubes under axial loading and external pressure

Y. Zhu *, X.Y. Luo, R.W. Ogden

Department of Mathematics, University of Glasgow, Glasgow G12 8QW, UK

Received 27 November 2007; received in revised form 2 February 2008
Available online 14 February 2008

Abstract

In this paper, we consider bifurcation from a circular cylindrical deformed configuration of a thick-walled circular cylindrical tube of incompressible isotropic elastic material subject to combined axial loading and external pressure. In particular, we examine both axisymmetric and asymmetric modes of bifurcation. The analysis is based on the three-dimensional incremental equilibrium equations, which are derived and then solved numerically for a specific material model using the Adams–Moulton method. We assess the effects of wall thickness and the ratio of length to (external) radius on the bifurcation behaviour.

Keywords: Elastic stability; Finite deformation; Bifurcation; Elastic tube

1. Introduction

The stability of elastic shells has been analyzed over the course of the past century since the initial work on the topic by von Mises (1914), who derived an equation for the buckling pressure of a thin-walled elastic tube. This gives the pressure as proportional to the cube of the ratio of wall thickness to mean diameter. Since then buckling of circular cylindrical tubes under external pressure based has been studied extensively, for instance by Batdorf (1947), Nash (1954) and Flügge (1973). In these studies, a simple one-term deflection function was used and the problem was solved under special boundary conditions. More accurate solutions were obtained by Ho and Cheng (1963), Sobel (1964) and Yamaki (1969) for a variety of loading and boundary conditions where the pre-buckling state was given in terms of membrane theory. The same problem was then treated by Yamaki (1970) but with pre-buckling effects. His key finding was that the mode number of the most unstable mode increases as the tube length is decreased, and for a sufficiently long tube mode 2 bifurcation is the most unstable mode. The length of the tube at which the transition between the higher mode and mode 2 occurs, however, depends on the thickness ratio; the thicker the tube the shorter the length for which mode 2 becomes

* Corresponding author.
E-mail address: yzhu2009@googlemail.com (Y. Zhu).

0020-7683/$ - see front matter © 2008 Elsevier Ltd. All rights reserved.
doi:10.1016/j.ijsolstr.2008.02.005

the most unstable mode (Yamaki, 1984). Good agreement between these studies and various experiments (e.g., Weissman and Mockros, 1967) have led to the buckling prediction for a cylindrical tube being regarded as a solved problem (at least for thin shells).

Cylindrical tube bifurcation under external pressure is of interest not only in solid mechanics applications but it is also of great interest in the biomechanics context, specifically for the analysis of flow in tubes that leads to collapse. There is a whole range of fascinating dynamic behaviour, as exemplified by Bertram (1982, 1995), Bertram et al. (1990), Luo and Pedley (1996, 1998, 2000), Bertram and Elliot (2003) and Luo et al. (2008). With different emphases, related extensive studies on stabilities of circular cylindrical shells have also been carried out. Some of these, concerning geometrically non-linear vibrations and dynamics of circular cylindrical shells, were reviewed by Amabili and Païdoussis (2003), with and without fluid–structure intersections. Other recent advances in post-buckling analysis of thin-walled structures were reported by Kounadis (2006). With a particular interest in post-buckling behaviour Heil and Pedley (1996) examined the stability of cylindrical shells under external pressure using a geometrically non-linear shell theory and confirmed that the mode number of the most unstable mode increases as the tube length is decreased, as predicted by Yamaki (1984). Heil and Pedley (1996) also found that the bifurcation is not significantly affected by the presence of a full fluid–solid coupling (as long as the critical loading is the same), although the subsequent post-buckling behaviour can be very different with and without the internal flow. There is also an extensive literature on plastic buckling of circular tubes. Experimental and modelling aspects of the compression of steel tubes in the plastic regime have been reviewed in the recent works by Bardi and Kyriakides (2006) and Bardi et al. (2006), and we refer to these papers for references to the relevant literature.

In experimental studies for these kinds of problems the tube wall thickness typically exceeds that which might be appropriate for thin-shell theories (Bertram, 1982, 1987; Bertram et al., 1990). It is therefore reasonable to ask if the bifurcation predictions of the classical theories remain valid. Bertram (1987) studied experimentally the effects of wall thickness on the collapse of tubes and obtained agreement with the results of Weissman and Mockros (1967). In Bertram's study, wall thickness ratio h/R values used were 0.38 and 0.5, where h is the thickness and R is the internal radius. The thick-walled tube problem was also analyzed by Marzo et al. (2005) using the finite element method, and good agreement with the experiments of Bertram (1987) and Weissman and Mockros (1967) was achieved. However, in Bertram (1987) and Marzo et al. (2005) results were presented only for mode 2 bifurcation and for limited values of the wall thickness. Therefore, it remains unclear how far the bifurcation predictions of thin-shell theory can be extended to thick-walled tubes, for which non-linear elastic deformations can no longer be neglected.

For problems involving non-linear elastic deformations, a rigorous bifurcation theory has been established based on the analysis of infinitesimal deformations superimposed on a known large deformation (Green et al., 1952). Using this theory, Nowinski and Shahinpoor (1969) examined the stability of an infinitely long circular cylinder of neo-Hookean material under external pressure assuming a plane strain deformation, and Wang and Ertepinar (1972) investigated the stability of infinitely long cylindrical shells and spherical shells subjected to both internal and external pressure. On the same basis but for different (incompressible, isotropic) material models Haughton and Ogden (1979b) examined in some detail the bifurcation behaviour of circular cylindrical tubes of finite length under *internal* pressure and axial loading.

In the present paper, following the analysis of Haughton and Ogden (1979b), we consider the bifurcation of incompressible, isotropic thick-walled circular cylindrical tubes of finite length when subject to both axial loading and external pressure. A new feature of the present work is the combination of finite deformations of thick-walled tubes of hyperelastic material with *external* pressure and axial loading.

In Section 2 we summarize the necessary equations that describe finite elastic deformations, while in Section 3 these are specialized to the circular cylindrical geometry of a thick-walled tube that maintains its circular cylindrical shape under axial extension and external pressure. The equations that describe a general (three-dimensional) incremental deformation superimposed on the deformed circular cylindrical tube are then given in Section 4. The three coupled partial differential equations governing the incremental displacement components are highlighted in Section 5 along with the relevant incremental boundary conditions. Based on an appropriate Ansatz for the displacement components the equations reduce to coupled ordinary differential equations, for the solution of which a numerical scheme is then described. In Section 6 the numerical method

is used in respect of a specific material model in order to obtain details of the onset of bifurcation in either an axisymmetric or asymmetric mode.

For the thinner tubes it is found that under external pressure axisymmetric bifurcation occurs only for $0 < \lambda_z < 1$, where λ_z is the principal stretch in the axial direction of the finite deformation. Moreover, the trend of the bifurcation curves is very different from that of a tube under internal pressure. Since externally pressurized tubes are particularly prone to asymmetric bifurcations, we devote most of our effort to the study of asymmetric bifurcations. The bifurcation modes are characterized by azimuthal mode number m and the tube length (which can be taken as a proxy for the axial mode number n). The bifurcation curves for modes $m = 1$ to $m = 4$ are presented, and the effects of wall thickness and the ratio of tube length to external radius on the buckling pressure are also examined. For the simpler cases, our results are in agreement with the published results in Marzo et al. (2005), Weissman and Mockros (1967), Bertram (1987) and Wang and Ertepinar (1972), and, in particular, with the von Mises equation (von Mises, 1914; Weissman and Mockros, 1967). We observe that the von Mises equation can only predict the buckling pressure well for thin shells. By contrast, the general analysis of bifurcation based on 3D finite deformation elasticity theory presented herein is valid for both thin and thick shells.

2. Basic equations

2.1. Deformation and equilibrium

Consider a deformable continuous body for which we take $\mathbf{X}$ to be the position vector of an arbitrary material point in the reference configuration, which is assumed to be stress free. Similarly, in the current configuration, let $\mathbf{x}$ be the position vector of the same material point. Suppose that the initial deformation is defined by the vector function $\boldsymbol{\chi}$, so that $\mathbf{x} = \boldsymbol{\chi}(\mathbf{X})$. Then the deformation gradient tensor $\mathbf{F}$ is defined by

$$\mathbf{F} = \operatorname{Grad} \boldsymbol{\chi}(\mathbf{X}). \tag{1}$$

At this point we do not need to express this in component form. The local ratio of current to reference volume is

$$J = \det \mathbf{F} > 0, \tag{2}$$

and for an incompressible material the constraint

$$J = \det \mathbf{F} \equiv 1 \tag{3}$$

must be satisfied for every material point $\mathbf{X}$.

We note that $\mathbf{F}$ can be written uniquely in the form $\mathbf{F} = \mathbf{RU}$, where $\mathbf{R}$ is a proper orthogonal tensor and $\mathbf{U}$ is positive definite and symmetric, the so-called right stretch tensor. The eigenvalues of $\mathbf{U}$ are the (strictly positive) principal stretches of the deformation, denoted λ_i, $i = 1, 2, 3$.

Let $\mathbf{S}$ denote the nominal stress tensor, which, in general, is not symmetric. Then, if there are no body forces the local equilibrium equation for the body has the (Lagrangian) form

$$\operatorname{Div} \mathbf{S} = \mathbf{0}. \tag{4}$$

The corresponding Cauchy stress tensor, denoted $\boldsymbol{\sigma}$, is related to $\mathbf{S}$ by $\boldsymbol{\sigma} = J^{-1}\mathbf{FS}$, is symmetric, and satisfies the Eulerian form of the equilibrium equation, namely

$$\operatorname{div} \boldsymbol{\sigma} = \mathbf{0}. \tag{5}$$

2.2. The elastic constitutive law and strain-energy function

We consider the material body to be composed of an elastic material, whose properties are described in terms of a strain-energy function, which we denote by $W = W(\mathbf{F})$ per unit reference volume. Here we confine attention to incompressible materials, so that the stress deformation relation is given by either

$$\mathbf{S} = \frac{\partial W}{\partial \mathbf{F}} - p\mathbf{F}^{-1}, \tag{6}$$

where p (an arbitrary hydrostatic stress) is a Lagrange multiplier associated with the constraint (3), or

$$\boldsymbol{\sigma} = \mathbf{F}\frac{\partial W}{\partial \mathbf{F}} - p\mathbf{I}, \tag{7}$$

where $\mathbf{I}$ is the identity tensor.

Here we take the material to be isotropic, so that W depends on $\mathbf{F}$ only through the principal stretches λ_i, $i = 1, 2, 3$, and is a symmetric function of the stretches. We therefore represent W in the form $W = W(\lambda_1, \lambda_2, \lambda_3)$, and, for an incompressible material, the constraint (3) may be written in terms of the stretches as

$$\lambda_1\lambda_2\lambda_3 = 1. \tag{8}$$

Moreover, (7) can be decomposed on principal axes as

$$\sigma_i = \lambda_i \frac{\partial W}{\partial \lambda_i} - p, \quad i = 1, 2, 3 \text{ (no summation)}, \tag{9}$$

σ_i, $i = 1, 2, 3$, being the principal Cauchy stresses.

For subsequent convenience it is useful to regard W as a function of just two independent stretches, λ_1 and λ_2 say, and to introduce the notation $\widehat{W}$ defined by

$$\widehat{W}(\lambda_1, \lambda_2) = W(\lambda_1, \lambda_2, \lambda_1^{-1}\lambda_2^{-1}). \tag{10}$$

It then follows from (9) that the principal stress differences can be written

$$\sigma_1 - \sigma_3 = \lambda_1 \frac{\partial \widehat{W}}{\partial \lambda_1}, \quad \sigma_2 - \sigma_3 = \lambda_2 \frac{\partial \widehat{W}}{\partial \lambda_2}. \tag{11}$$

3. The circular cylindrical configuration

We now consider a thick-walled circular cylindrical tube with reference geometry described by

$$A \leqslant R \leqslant B, \quad 0 \leqslant \Theta \leqslant 2\pi, \quad 0 \leqslant Z \leqslant L, \tag{12}$$

where R, Θ, Z are cylindrical polar coordinates, A and B are the inner and outer radii, respectively, and L is the length of the tube. This is depicted in Fig. 1(a).

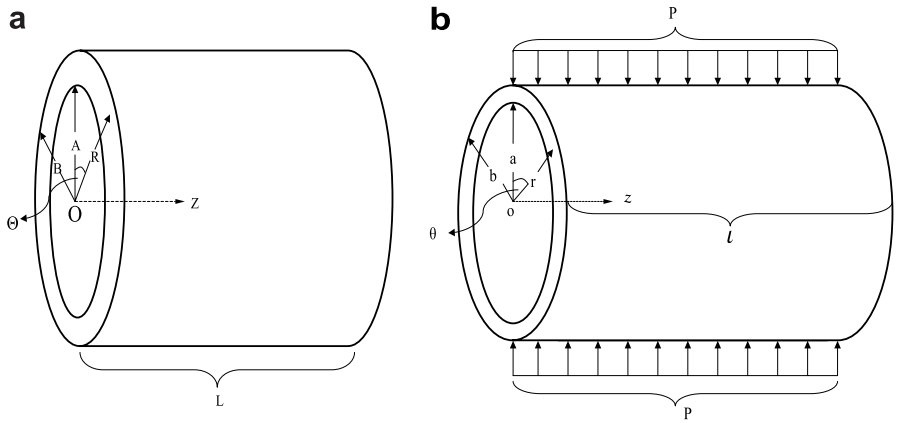

Fig. 1. The circular cylindrical tube in its reference configuration (a) and deformed configuration when subject to axial load and external pressure (b).

The initial deformed configuration of the tube, under the action of axial loading and external pressure, is assumed also to be circular cylindrical, with geometry described by

$$a \leqslant r \leqslant b, \quad 0 \leqslant \theta \leqslant 2\pi, \quad 0 \leqslant z \leqslant l, \tag{13}$$

where r, θ, z are cylindrical polar coordinates, a and b are the internal and external radii, respectively, and l is the length. Since the material is incompressible, the deformation is described by the equations

$$r^2 = a^2 + \lambda_z^{-1}(R^2 - A^2), \quad \theta = \Theta, \quad z = \lambda_z Z, \tag{14}$$

where λ_z is the axial extension ratio (or axial stretch), which is uniform.

We use $\mathbf{e}_1, \mathbf{e}_2, \mathbf{e}_3$ to denote the unit basis vectors corresponding to the coordinates θ, z, r, respectively. For the considered deformation, since the material is isotropic, these define the principal directions of both the stretch tensor $\mathbf{U}$ and the Cauchy stress $\boldsymbol{\sigma}$. Let $\lambda_1, \lambda_2, \lambda_3$ denote the corresponding principal stretches and $\sigma_1, \sigma_2, \sigma_3$ the associated principal Cauchy stresses, which are given by (9). From the incompressibility constraint together with (14), we have

$$\lambda_2 = \lambda_z, \quad \lambda_1 = \frac{r}{R} \equiv \lambda, \quad \lambda_3 = (\lambda_1 \lambda_z)^{-1}. \tag{15}$$

For the symmetric configuration considered here, the only equilibrium equation not satisfied trivially is

$$r\frac{d\sigma_3}{\mathrm{d}r} + \sigma_3 - \sigma_1 = 0, \tag{16}$$

and we have the associated boundary conditions

$$\sigma_3 = \begin{cases} 0 & \text{on } r = a \\ -P & \text{on } r = b. \end{cases} \tag{17}$$

Using $\widehat{W}$, as defined in (10), $(11)_1$, and the definitions (15), integration of (16) and application of the boundary conditions (17) yields

$$P = -\int_a^b \lambda \widehat{W}_\lambda \frac{\mathrm{d}r}{r}. \tag{18}$$

On application of the connections $r = \lambda R$ and (14) this may be re-written with λ as the integration variable in the form

$$P = \int_{\lambda_a}^{\lambda_b} \frac{\widehat{W}_\lambda}{(\lambda^2 \lambda_z - 1)} \mathrm{d}\lambda, \tag{19}$$

where

$$\lambda_a = \frac{a}{A}, \quad \lambda_b = \frac{b}{B}. \tag{20}$$

We note here that if there is, additionally, an internal pressure, $P_i > 0$ say, then the left-hand sides of (18) and (19) are replaced by $P - P_i$. Thus, the effect of an internal pressure can be captured by taking $P < 0$ in the above formulas, this corresponding to a radial external tension on $r = b$.

4. Incremental equations

Detailed derivation of the incremental equations can be found in Haughton and Ogden (1979b) for a thick-walled and Haughton and Ogden (1979a) for a thin-walled tube (see also Haughton and Ogden, 1978a,b, for corresponding results for spherical shells). Here we provide a summary of the main results needed for our analysis. A superposed dot signifies an increment in the quantity concerned, and a subscript 0 indicates that the quantity to which it is attached is calculated with respect to the deformed configuration as reference configuration. First, let $\dot{\mathbf{x}}(\mathbf{X})$ denote the incremental displacement vector, and then define $\mathbf{u}(\mathbf{x})$ through $\mathbf{u}(\mathbf{x}) = \mathbf{u}(\boldsymbol{\chi}(\mathbf{X})) = \dot{\mathbf{x}}(\mathbf{X})$. Next, introduce the notation $\boldsymbol{\eta}$ defined by

$$\boldsymbol{\eta} = \dot{\mathbf{F}}_0 \equiv \dot{\mathbf{F}}\mathbf{F}^{-1} = \operatorname{grad}\mathbf{u}. \tag{21}$$

The incremental form of the incompressibility condition can then be written

$$\operatorname{tr}\boldsymbol{\eta} = 0. \tag{22}$$

The increment of the constitutive law (6) has the form

$$\dot{\mathbf{S}} = \boldsymbol{\mathcal{A}}\dot{\mathbf{F}} - \dot{p}\mathbf{F}^{-1} + p\mathbf{F}^{-1}\dot{\mathbf{F}}\mathbf{F}^{-1}, \tag{23}$$

where

$$\boldsymbol{\mathcal{A}} = \frac{\partial^2 W}{\partial\mathbf{F}\partial\mathbf{F}} \tag{24}$$

is the elasticity tensor with components defined by

$$\mathcal{A}_{\alpha i\beta j} = \frac{\partial^2 W}{\partial F_{i\alpha}\partial F_{j\beta}}. \tag{25}$$

When the reference configuration is updated to the current configuration this becomes

$$\dot{\mathbf{S}}_0 = \boldsymbol{\mathcal{B}}\boldsymbol{\eta} + p\boldsymbol{\eta} - \dot{p}\mathbf{I}, \tag{26}$$

where $\mathbf{I}$ is again the identity tensor and $\boldsymbol{\mathcal{B}}$ is the fourth-order tensor of instantaneous elastic moduli, whose (Cartesian) components are related to those of $\boldsymbol{\mathcal{A}}$ by

$$\mathcal{B}_{piqj} = F_{p\alpha}F_{q\beta}\mathcal{A}_{\alpha i\beta j}. \tag{27}$$

For an incompressible isotropic elastic material the non-vanishing components of $\boldsymbol{\mathcal{B}}$ referred to the principal axes of $\boldsymbol{\sigma}$ can be written (see, for example, Ogden, 1974)

$$\mathcal{B}_{iijj} = \mathcal{B}_{jjii} = \lambda_i\lambda_j W_{ij}, \tag{28}$$

$$\mathcal{B}_{ijij} = \frac{\lambda_i W_i - \lambda_j W_j}{\lambda_i^2 - \lambda_j^2}\lambda_i^2, \quad \lambda_i \neq \lambda_j, \tag{29}$$

$$\mathcal{B}_{ijji} = \mathcal{B}_{jiij} = \mathcal{B}_{ijij} - \lambda_i W_i, \quad i \neq j, \tag{30}$$

where $W_i = \partial W/\partial\lambda_i$, $W_{ij} = \partial^2 W/\partial\lambda_i\partial\lambda_j$.

The incremental form of the equilibrium Eq. (4) is $\operatorname{Div}\dot{\mathbf{S}} = \mathbf{0}$ and when updated it becomes

$$\operatorname{div}\dot{\mathbf{S}}_0 = \mathbf{0}, \tag{31}$$

the incremental counterpart of (5).

For the problem to be considered in the following sections we shall be making use of the pressure boundary condition, which, referred to the original reference configuration, may be written

$$\mathbf{S}^{\mathrm{T}}\mathbf{N} = -P\mathbf{F}^{-\mathrm{T}}\mathbf{N}, \tag{32}$$

where $\mathbf{N}$ is the unit outward normal vector to the boundary of the body in the reference configuration and P is the pressure on the boundary per unit area of the deformed configuration. On taking the increment of (32) and updating to the deformed configuration we obtain

$$\dot{\mathbf{S}}_0^{\mathrm{T}}\mathbf{n} = P\boldsymbol{\eta}^{\mathrm{T}}\mathbf{n} - \dot{P}\mathbf{n}, \tag{33}$$

which is the form of incremental boundary condition that we shall use.

We now specialize (31) to circular cylindrical coordinates based of the underlying solution discussed in Section 3. The curvilinear coordinates are ordered so that $(x^1, x^2, x^3) = (\theta, z, r)$. Then, we have, in component form,

$$\dot{S}_{0ji,j} + \dot{S}_{0ji}\mathbf{e}_k \cdot \mathbf{e}_{j,k} + \dot{S}_{0kj}\mathbf{e}_i \cdot \mathbf{e}_{j,k} = 0, \quad i = 1, 2, 3, \tag{34}$$

with summation over indices j and k from 1 to 3, where the subscript $j(=1, 2, 3)$ following a comma represents the derivatives $(\partial/r\partial\theta, \partial/\partial z, \partial/\partial r)$. The only non-zero components of $\mathbf{e}_i \cdot \mathbf{e}_{j,k}$ are

$$\mathbf{e}_1 \cdot \mathbf{e}_{3,1} = \frac{1}{r}, \quad \mathbf{e}_3 \cdot \mathbf{e}_{1,1} = -\frac{1}{r}. \tag{35}$$

Referred to the cylindrical polar axes the incremental displacement $\mathbf{u}$ is written in terms of its components (v, w, u) as

$$\mathbf{u} = v\mathbf{e}_1 + w\mathbf{e}_2 + u\mathbf{e}_3. \tag{36}$$

Then, from the definition $\boldsymbol{\eta} = \operatorname{grad}\mathbf{u}$ we obtain the component matrix of $\boldsymbol{\eta}$ referred to the axes in question as

$$[\boldsymbol{\eta}] = \begin{pmatrix} (u+v_\theta)/r & v_z & v_r \\ w_\theta/r & w_z & w_r \\ (u_\theta - v)/r & u_z & u_r \end{pmatrix}, \tag{37}$$

where the square brackets indicate the matrix of components of the enclosed quantity and the subscripts (r, θ, z) signify standard partial derivatives.

The incompressibility condition (22) can now be given explicitly as

$$\operatorname{tr}\boldsymbol{\eta} \equiv u_r + (u + v_\theta)/r + w_z = 0. \tag{38}$$

5. Asymmetric bifurcations and numerical methods

We now substitute (26), (37), (38) and the expressions for the components of $\mathcal{B}_{ijkl}$ into (34) to obtain

$$\begin{aligned}\dot{p}_\theta &= (r\mathcal{B}'_{3131} + \mathcal{B}_{3131})(u_\theta + rv_r - v)/r + (\mathcal{B}_{1111} - \mathcal{B}_{1122} - \mathcal{B}_{2112})(u_\theta + v_{\theta\theta})/r \\ &\quad + \mathcal{B}_{2121} r v_{zz} + \mathcal{B}_{3131} r v_{rr} + (\mathcal{B}_{1133} - \mathcal{B}_{1122} - \mathcal{B}_{2112} + \mathcal{B}_{3113}) u_{r\theta}, \end{aligned} \tag{39}$$

$$\begin{aligned}\dot{p}_z &= (r\mathcal{B}'_{3232} + \mathcal{B}_{3232})(u_z + w_r)/r + \mathcal{B}_{1212}(w_{\theta\theta} - ru_z)/r^2 + \mathcal{B}_{3232} w_{rr} \\ &\quad + (\mathcal{B}_{2222} - \mathcal{B}_{1221} - \mathcal{B}_{1122}) w_{zz} + (\mathcal{B}_{2233} + \mathcal{B}_{3223} - \mathcal{B}_{1221} - \mathcal{B}_{1122}) u_{rz}, \end{aligned} \tag{40}$$

$$\begin{aligned}\dot{p}_r &= (r\mathcal{B}'_{1133} - r\mathcal{B}'_{2233} - \mathcal{B}_{1111} + \mathcal{B}_{1122})(u + v_\theta)/r^2 + \mathcal{B}_{1313}(u_{\theta\theta} - v_\theta)/r^2 + \mathcal{B}_{3223} w_{rz} \\ &\quad + (\mathcal{B}_{1331} + \mathcal{B}_{1133} - \mathcal{B}_{2233}) v_{r\theta}/r + (\mathcal{B}_{3333} - \mathcal{B}_{2233}) u_{rr} + \mathcal{B}_{2323} u_{zz} \\ &\quad + (r\mathcal{B}'_{3333} + rp' - r\mathcal{B}'_{2233} + \mathcal{B}_{3333} - 2\mathcal{B}_{2233} + \mathcal{B}_{1122}) u_r/r. \end{aligned} \tag{41}$$

On the cylindrical boundaries we apply the specialization of (33) to the present situation, with the inner boundary free of incremental traction and the outer boundary subject to pressure P. Taking $\dot{P} = 0$ in (33) we then have, for $i = 1, 2, 3$,

$$\dot{S}_{03i} = \begin{cases} 0 & \text{on } r = a \\ P\eta_{3i} & \text{on } r = b. \end{cases} \tag{42}$$

At the ends of the tube we apply the incremental boundary conditions

$$u = v = 0, \quad \dot{S}_{022} = 0 \quad \text{on } z = 0, l. \tag{43}$$

This means that the ends of the tube are constrained so that no incremental rotation or radial displacement is allowed, while the axial component of traction is of dead-load type.

To solve the equations, we assume that the solution takes the form

$$\left.\begin{aligned} u &= f(r)\cos m\theta \sin \alpha z, \quad & v &= g(r)\sin m\theta \sin \alpha z, \\ w &= h(r)\cos m\theta \cos \alpha z, \quad & \dot{p} &= k(r)\cos m\theta \sin \alpha z, \end{aligned}\right\} \tag{44}$$

where $m = 0, 1, 2, 3, \ldots$ is the azimuthal mode number, $m = 0$ corresponding to an axisymmetric solution. Substitution into the incompressibility condition (38) then yields

$$rf'(r) + f(r) + mg(r) - \alpha r h(r) = 0. \tag{45}$$

Also, on inserting (44) into (39)–(41) and using (45) to eliminate $h(r)$, we obtain three coupled equations for $f(r), g(r)$ and $k(r)$, namely

$$(r\mathcal{B}'_{3131}+\mathcal{B}_{3131}+\mathcal{B}_{1111}-\mathcal{B}_{1122}-\mathcal{B}_{2112})mf(r)+(\mathcal{B}_{1133}-\mathcal{B}_{1122}+\mathcal{B}_{3113}-\mathcal{B}_{2112})mrf'(r)$$
$$+[r\mathcal{B}'_{3131}+\mathcal{B}_{3131}+m^2(\mathcal{B}_{1111}-\mathcal{B}_{1122}-\mathcal{B}_{2112})+\alpha^2r^2\mathcal{B}_{2121}]g(r)$$
$$-(r\mathcal{B}'_{3131}+\mathcal{B}_{3131})rg'(r)-\mathcal{B}_{3131}r^2g''(r)-mrk(r)=0, \tag{46}$$

$$[r\mathcal{B}'_{3232}-\mathcal{B}_{3232}+m^2\mathcal{B}_{1212}-\alpha^2r^2(r\mathcal{B}'_{3232}+\mathcal{B}_{3232}-\mathcal{B}_{1212}+\mathcal{B}_{1122}+\mathcal{B}_{1221}-\mathcal{B}_{2222})]f(r)$$
$$-[r\mathcal{B}'_{3232}-\mathcal{B}_{3232}-m^2\mathcal{B}_{1212}-\alpha^2r^2(\mathcal{B}_{2222}-\mathcal{B}_{2233}-\mathcal{B}_{3223})]rf'(r)$$
$$-(r\mathcal{B}'_{3232}+2\mathcal{B}_{3232})r^2f''(r)-\mathcal{B}_{3232}r^3f'''(r)+[r\mathcal{B}'_{3232}-\mathcal{B}_{3232}+m^2\mathcal{B}_{1212}$$
$$+\alpha^2r^2(\mathcal{B}_{2222}-\mathcal{B}_{1122}-\mathcal{B}_{1221})]mg(r)-(r\mathcal{B}'_{3232}-\mathcal{B}_{3232})mrg'(r)-\mathcal{B}_{3232}mr^2g''(r)+\alpha^2r^3k(r)=0, \tag{47}$$

$$(r\mathcal{B}'_{1133}-r\mathcal{B}'_{2233}-\mathcal{B}_{1111}+\mathcal{B}_{1122}+\mathcal{B}_{3223}-m^2\mathcal{B}_{1313}-\alpha^2r^2\mathcal{B}_{2323})f(r)$$
$$+(r\mathcal{B}'_{3333}+rp'-r\mathcal{B}'_{2233}+\mathcal{B}_{3333}-2\mathcal{B}_{2233}+\mathcal{B}_{1122}-\mathcal{B}_{3223})rf'(r)$$
$$+(\mathcal{B}_{3333}-\mathcal{B}_{2233}-\mathcal{B}_{3223})r^2f''(r)+(r\mathcal{B}'_{1133}-r\mathcal{B}'_{2233}-\mathcal{B}_{1111}+\mathcal{B}_{1122}+\mathcal{B}_{3223}-\mathcal{B}_{1313})mg(r)$$
$$+(\mathcal{B}_{1133}-\mathcal{B}_{2233}+\mathcal{B}_{1331}-\mathcal{B}_{3223})mrg'(r)-r^2k'(r)=0. \tag{48}$$

Next, on substituting the expression for u from (44) in the boundary condition $(43)_1$, we deduce that

$$\alpha=n\pi/(\lambda_2L), \tag{49}$$

where $n=1,2,3,\ldots$ is the axial mode number. The boundary conditions for v are then automatically satisfied. It is therefore clear that the behaviour for different mode numbers n can be captured, equivalently, by varying the length L. Thus, in what follows it suffices to set $n=1$ and to consider L as a parameter that reflects either changes in the axial mode number or changes in length.

From Eqs. (46)–(48), we can express $f'''(r)$, $g''(r)$ and $k'(r)$ in terms of $f(r)$, $f'(r)$, $f''(r)$, $g(r)$, $g'(r)$ and $k(r)$, and hence we write the equations as a first-order system in the compact form

$$\frac{d\mathbf{y}}{\mathrm{d}r}=\mathbf{G}(\mathbf{y},r), \tag{50}$$

where $\mathbf{y}=(y_1,y_2,y_3,y_4,y_5,y_6)^{\mathrm{T}}$, $\mathbf{G}=(G_1,G_2,G_3,G_4,G_5,G_6)^{\mathrm{T}}$,

$$y_1=f(r),\quad y_2=f'(r),\quad y_3=f''(r),\quad y_4=g(r),\quad y_5=g'(r),\quad y_6=k(r), \tag{51}$$

and

$$G_1=y_2,\quad G_2=y_3,\quad G_4=y_5, \tag{52}$$

while G_3, G_5, G_6 are lengthy expressions obtained by rearranging Eqs. (46)–(48) and are not listed here.

In the same notation, the components of the incremental pressure boundary condition (33) are given as

$$\left.\begin{aligned}&my_1+y_4-ry_5=0,\\&(\alpha^2r^2+m^2-1)y_1+ry_2+r^2y_3=0,\\&(\mathcal{B}_{1133}-\mathcal{B}_{2233})(y_1+my_4)+(\mathcal{B}_{3333}-\mathcal{B}_{2233}+\lambda_3W_3)ry_2-ry_6=0,\end{aligned}\right\} \tag{53}$$

each of which must hold on both $r=a$ and $r=b$. To obtain these use has been made of the conditions $\sigma_3=\lambda_3W_3-p=0$ on $r=a$ and $\sigma_3=\lambda_3W_3-p=-P$ on $r=b$, and we have set $\dot{P}=0$ on $r=b$.

To solve the system of first-order ordinary differential equations (with three independent solutions), we choose starting values at $r=a$ for three independent solutions given by

$$\begin{pmatrix}y_1^1(a)&y_1^2(a)&y_1^3(a)\\y_4^1(a)&y_4^2(a)&y_4^3(a)\\y_6^1(a)&y_6^2(a)&y_6^3(a)\end{pmatrix}=\begin{pmatrix}1&0&0\\0&1&0\\0&0&1\end{pmatrix}, \tag{54}$$

where, for each entry $y_i^j(a)$ in (54), subscripts $i=1,4,6$, correspond to dependent variables in (50) while the superscript j refers to the jth set of initial values ($j=1,2,3$).

Substituting each set of the initial values, that is each column of the matrix (54), into the boundary conditions (53) for $r=a$, we obtain

$$\begin{pmatrix} y_2^1(a) & y_2^2(a) & y_2^3(a) \\ y_3^1(a) & y_3^2(a) & y_3^3(a) \\ y_5^1(a) & y_5^2(a) & y_5^3(a) \end{pmatrix} = \begin{pmatrix} a_{11} & my_2^1(a) & a_{13} \\ a_{21} & -my_2^1(a)/a & -y_2^3(a)/a \\ m/a & 1/a & 0 \end{pmatrix}, \tag{55}$$

where, for conciseness, we have introduced the notations

$$a_{11} = \frac{\mathcal{B}_{2233} - \mathcal{B}_{1133}}{a(\mathcal{B}_{3333} - \mathcal{B}_{2233} + \lambda_3 W_3)}, \quad a_{13} = \frac{1}{\mathcal{B}_{3333} - \mathcal{B}_{2233} + \lambda_3 W_3}, \quad a_{21} = \frac{1 - m^2 - a^2\alpha^2 - ay_2^1(a)}{a^2},$$

all terms being evaluated for $r = a$.

Eqs. (54) and (55) together give the initial values for Eq. (50). This initial value problem is solved numerically using the Adams–Moulton method (Gerald and Wheatley, 1984), with Predictor and Corrector given by

$$\text{Predictor} : \mathbf{y}_{n+1} = \mathbf{y}_n + \frac{h}{24}(55\mathbf{G}_n - 59\mathbf{G}_{n-1} + 37\mathbf{G}_{n-2} - 9\mathbf{G}_{n-3}), \tag{56}$$

$$\text{Corrector} : \mathbf{y}_{n+1} = \mathbf{y}_n + \frac{h}{24}(9\mathbf{G}_{n+1} + 19\mathbf{G}_n - 5\mathbf{G}_{n-1} + \mathbf{G}_{n-2}), \tag{57}$$

where $h = (b-a)/\omega$ is the step size and ω is the iteration number. Note that the Adams–Moulton method requires four sets of initial values at previous steps. These are calculated using the fourth-order Runge–Kutta method. Each method has local errors of $O(h^5)$. The solutions can be expressed as a linear combination of the three independent solutions $\mathbf{y}^1, \mathbf{y}^2, \mathbf{y}^3$. Thus,

$$\mathbf{y} = C_1\mathbf{y}^1 + C_2\mathbf{y}^2 + C_3\mathbf{y}^3, \tag{58}$$

where $\mathbf{y}^i = (y_1^i, y_2^i, y_3^i, y_4^i, y_5^i, y_6^i)^{\mathrm{T}}, i = 1, 2, 3$.

Bifurcation may occur if there exist constants C_1, C_2, C_3, at least one of which is non-zero. For purposes of numerical computation in Section 6 we shall specialize to a particular strain-energy function, for which $\mathcal{B}_{1133} = \mathcal{B}_{2233} = 0$. On introducing this specialization and substituting (58) into the boundary conditions (53), we obtain three equations for C_1, C_2, C_3, namely

$$\left.\begin{aligned} &[my_1^i(b) + y_4^i(b) - by_5^i(b)]C_i = 0, \\ &[(m^2 + \alpha^2 b^2 - 1)y_1^i(b) + b(y_2^i(b) + by_3^i(b))]C_i = 0, \\ &[b(\mathcal{B}_{3333} + \lambda_3 W_3)y_2^i(b) - by_6^i(b)]C_i = 0, \end{aligned}\right\} \tag{59}$$

evaluated for $r = b$, in each of which there is summation over the index i from 1 to 3. Thus, the bifurcation criterion is obtained by the vanishing of the determinant of coefficients of C_1, C_2, C_3, viz.

$$\begin{vmatrix} my_1^1(b) + y_4^1(b) - by_5^1(b) & my_1^2(b) + y_4^2(b) - by_5^2(b) & my_1^3(b) + y_4^3(b) - by_5^3(b) \\ My_1^1(b) + by_2^1(b) + b^2y_3^1(b) & My_1^2(b) + by_2^2(b) + b^2y_3^2(b) & My_1^3(b) + by_2^3(b) + b^2y_3^3(b) \\ bNy_2^1(b) - by_6^1(b) & bNy_2^2(b) - by_6^2(b) & bNy_2^3(b) - by_6^3(b) \end{vmatrix} = 0, \tag{60}$$

again with all terms evaluated for $r = b$, where $M = m^2 + \alpha^2 b^2 - 1$ and $N = \mathcal{B}_{3333} + \lambda_3 W_3$.

Substituting the equation

$$b^2 = a^2 + \lambda_z^{-1}(B^2 - A^2), \tag{61}$$

i.e. Eq. $(14)_1$ with $R = B$, into (60), we obtain an equation for the value of a that satisfies the bifurcation criterion (60). The corresponding bifurcation pressure can be obtained from (19).

6. Numerical results and discussion

In the experiments of Weissman and Mockros (1967) and Bertram (1987) silicone rubber tubes were used, and the numerical results of Marzo et al. (2005) were compared with experimental data for two thick-walled collapsible tubes reported by Bertram (1987). It is therefore appropriate to employ a strain-energy function that has been used extensively for fitting data on experiments for a wide range of rubberlike solids. Specifically, we apply the foregoing theory to the strain-energy function given by

$$W = \sum_{r=1}^{3} \mu_r(\lambda_1^{\alpha_r} + \lambda_2^{\alpha_r} + \lambda_3^{\alpha_r} - 3)/\alpha_r, \tag{62}$$

where μ_r and α_r, $r = 1, 2, 3$, are material constants (see, for example, Ogden, 1997). Using the incompressibility condition (8) and the energy function $\widehat{W}(\lambda_1, \lambda_2)$ defined by (10), we have

$$\widehat{W}(\lambda_1, \lambda_2) = \sum_{r=1}^{3} \mu_r(\lambda_1^{\alpha_r} + \lambda_2^{\alpha_r} + (\lambda_1\lambda_2)^{-\alpha_r} - 3)/\alpha_r. \tag{63}$$

For the numerical calculations we use the material constants given by

$$\begin{aligned} &\alpha_1 = 1.3, \quad \alpha_2 = 5.0, \quad \alpha_3 = -2.0, \\ &\mu_1^* = 1.491, \quad \mu_2^* = 0.003, \quad \mu_3^* = -0.023, \end{aligned} \tag{64}$$

as in Haughton and Ogden (1978b), where $\mu_r^* = \mu_r/\mu$, $r = 1, 2, 3$, and μ is the shear modulus of the material in the reference configuration given by (see, for example, Ogden, 1972)

$$2\mu = \sum_{r=1}^{3} \mu_r\alpha_r. \tag{65}$$

Representative values of the aspect ratios of the tube are taken as $L/B = 1, 2.5, 5, 10$, and for numerical purposes, without loss of generality, we set $B = 1$ and change the value of the inner radius A to vary the thickness of the tube. Two thickness ratios are considered, namely, $A/B = 0.85$ (thinner tube) and $A/B = 0.5$ (thicker tube).

The qualitative nature of the results presented below are not unduly sensitive to the choice of material parameters in (62), and there are also many other forms of strain-energy function that could equally well be used to produce similar qualitative behaviour.

6.1. Equilibrium pressure curves

The dependence of the non-dimensional pressure $P^* = P/\mu$ on the circumferential stretch λ_a is illustrated in Fig. 2(a) in respect of the strain-energy function (63) with material constants (64) and for $A/B = 0.85$ and several values of λ_z. Fig. 2(a) shows that initially the external pressure increases slowly in order to compress the tube radially as λ_a is reduced from 1. Thereafter, there is a plateau where a significant increase in pressure does

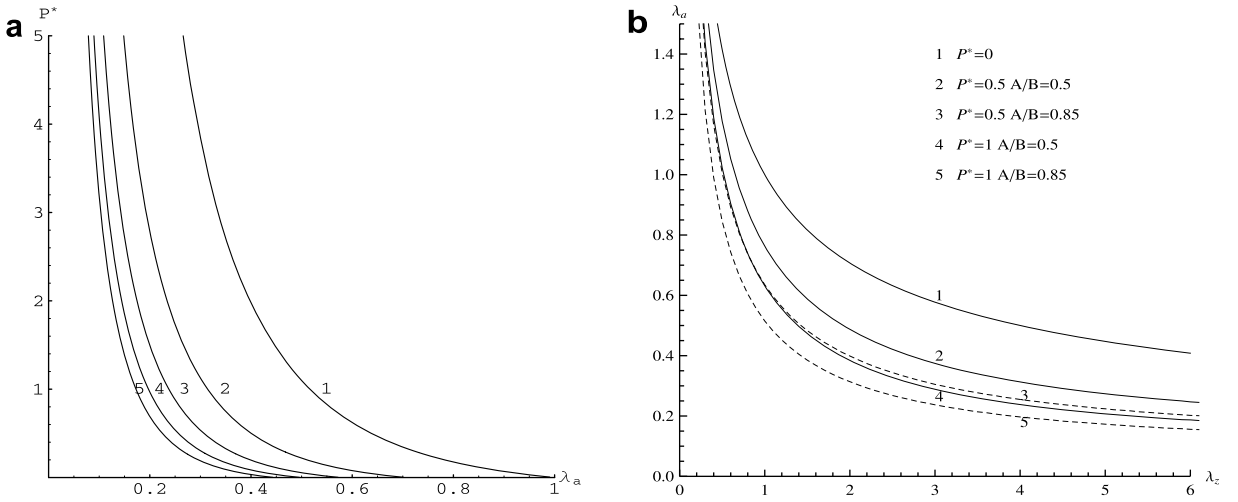

Fig. 2. Plot of (a) the dimensionless pressure $P^* = P/\mu$ against λ_a for $A/B = 0.85$ and $\lambda_z = 1, 2, 3, 4, 5$, and (b) equal pressure curves in (λ_z, λ_a) space for $P^* = 0, 0.5, 1$, with $A/B = 0.85$ (dashed curves) and $A/B = 0.5$ (continuous curves).

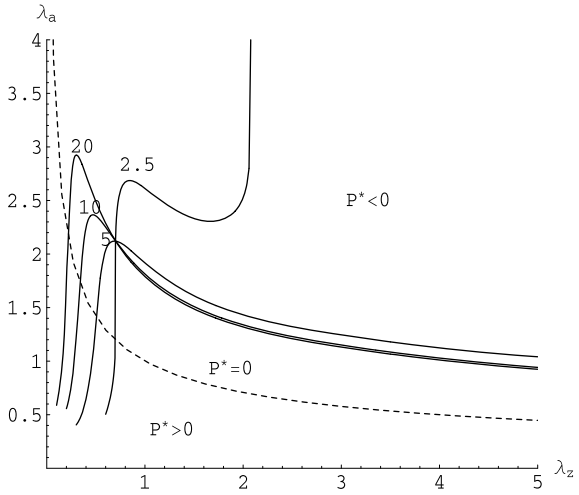

Fig. 3. Plots of the axisymmetric bifurcation curves for mode $n = 1$ with aspect ratios $L/B = 2.5, 5, 10, 20$ and $A/B = 0.85$. The dashed curve corresponds to the zero pressure curve $P^* = 0$.

not produce significant further radial deformation of the tube. This trend becomes more pronounced as the value of λ_z increases. This graph should be compared with the pressure-area (internal cross-sectional area of the tube) diagram, also known as the "tube law" and most commonly used for collapsible tubes (Flaherty et al., 1972). Although the tube law is based on the post-buckling behaviour of tubes it does not take account of axial forces and bending moments.

The equal pressure curves corresponding to $P^* = 0, 0.5, 1$ are plotted in (λ_z, λ_a) space for $A/B = 0.5$ and 0.85 in Fig. 2(b), again using Eq. (19), except for $P^* = 0$, for which we have the connection

$$\lambda_a^2 \lambda_z = 1, \tag{66}$$

which is independent of the wall thickness ratio A/B. We observe that at least for the range of values of λ_z and λ_a considered, the equal pressure curves for the thicker tube $(A/B = 0.5)$ lie above those for the thinner one $(A/B = 0.85)$, indicating that to obtain the same deformation more pressure is required for the thicker tube, as should be expected.

6.2. Axisymmetric bifurcation

First, we consider axisymmetric modes of bifurcation, corresponding to $m = 0$ in (44). We set the longitudinal mode number n to be 1 and in Fig. 3 we plot axisymmetric bifurcation curves for $L/B = 2.5, 5, 10$ and 20 and $A/B = 0.85$. In this case, as well as curves for an external pressure, curves for an internal pressure are shown in order to compare with the results of Haughton and Ogden (1979b). With reference to the remarks on internal pressure following Eq. (19), we recall that the effect of internal pressure is captured by taking $P^* < 0$ here. It can then be seen that for a tube subjected to internal pressure our results coincide with those in Haughton and Ogden (1979b) except for a factor 2, which means the curves in Haughton and Ogden (1979b) for $L/B = 2x$ are the same for those here with $L/B = x$.[1]

When the tube is under external pressure ($P^* > 0$), we note that the axisymmetric bifurcation curves all intersect the curve $P^* = 0$ in the region $0 < \lambda_z < 1$, which means that axisymmetric bifurcation cannot occur for tubes with $A/B = 0.85$ subjected to external pressure and axial extension (i.e. when $\lambda_z > 1$). In other words, under external pressure, axisymmetric bifurcation only occurs when a tube is axially compressed. This is not the case for tubes under internal pressure (Haughton and Ogden, 1979b).

[1] Private communication with Dr. Haughton confirms that there is a factor of 2 missing in Eq. (61) of Haughton and Ogden (1979b).

6.3. Asymmetric bifurcation

Since for tubes under external pressure, axisymmetric bifurcations do not occur when the tube is extended, we focus on asymmetric bifurcations henceforth.

6.3.1. Thinner tube

In this section, all results are for the thinner tube $A/B = 0.85$. From Eq. (49), we recall that either axial mode number n or length of the tube L can be varied to obtain equivalent results. We therefore set $n = 1$ and choose different values of the length L, and only azimuthal modes corresponding to $m = 1, 2, 3, 4$ are considered. Therefore, in the following, the mode number referred to is always the azimuthal mode number m. We restrict attention to $m \leqslant 4$ because higher mode number bifurcations are not usually observed in collapsible tube experiments. In any case, we have found that higher modes produce results very similar to those for $m = 4$. The asymmetric bifurcation curves are plotted using the bifurcation criterion (60) and the numerical method discussed in Section 5.

Fig. 4 shows the mode 1 asymmetric bifurcation curves for $L/B = 1, 2.5, 5, 10$ and both internal and external pressure. For $P^* < 0$ (tubes under internal pressure), the results here are again in agreement with those of Haughton and Ogden (1979b), with the factor 2 difference indicated earlier, and we do not discuss this case further. For $P^* > 0$ (tubes under external pressure), we see that as the axial stretch λ_z is increased towards 1, along the equal pressure curve $P^* = 0$ the value of λ_a at bifurcation decreases as the value of L/B increases from 2.5 to 10. This confirms the intuitive expectation that longer tubes buckle more easily than shorter ones. In the region of axial extension, the tube with $L/B = 1$ bifurcates slightly more readily into mode 1 than the longer tubes. Fig. 4 also shows that the tube can bifurcate into mode 1 for small axial compression (values of λ_z less than, but close to, 1). The value of λ_a at bifurcation seems to increase rapidly for λ_z below 1 (i.e. when the tube is axially compressed). However, under axial extension ($\lambda_z > 1$), bifurcation into mode 1 requires a relatively larger pressure than in axial compression and the corresponding value of λ_a becomes very small, as does the internal radius of the tube.

The mode 2 asymmetric bifurcation curves are shown in Fig. 5. It is interesting to see that the bifurcation pressure for longer tubes ($L/B \geqslant 5$) approaches zero. Thus, although the bifurcation pressures required in the region of axial compression are similar for mode 1 and mode 2, much less pressure is required to achieve the mode 2 bifurcation in the region of axial extension. Fig. 5 also shows that the mode 2 bifurcation does not depend significantly on the length of the tube unless the tube is very short (with L/B about 1).

Similar bifurcation behaviour is found for modes $m = 3$ and $m = 4$, as illustrated in Fig. 6. Compared with mode 2, the mode 3 and mode 4 curves are closer to (further from) the equal pressure line $P^* = 0$ for tubes with $L/B = 1$ ($L/B = 10$), and hence the shorter tubes become more sensitive to a change in the external pres-

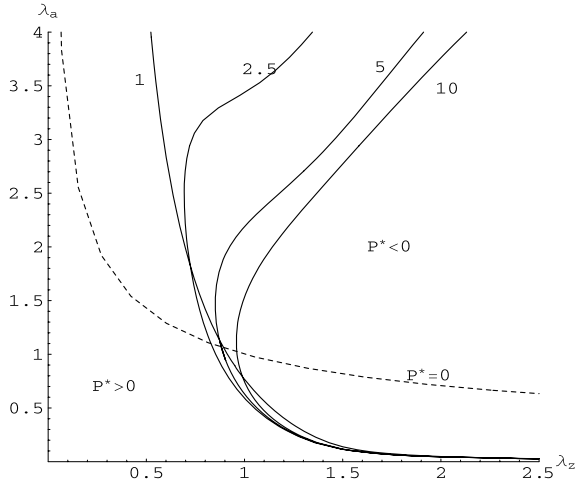

Fig. 4. Mode $m = 1$ asymmetric bifurcation curves for $L/B = 1, 2.5, 5, 10$ and $A/B = 0.85$ in (λ_z, λ_a) space. The dashed curve is the equal pressure curve $P^* = 0$.

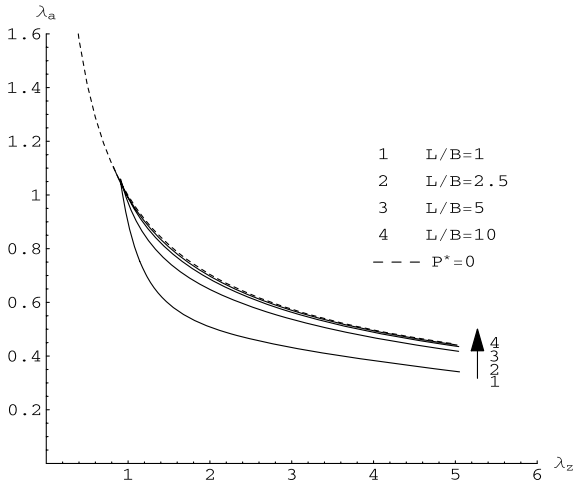

Fig. 5. As in Fig. 4 but for azimuthal mode number $m = 2$.

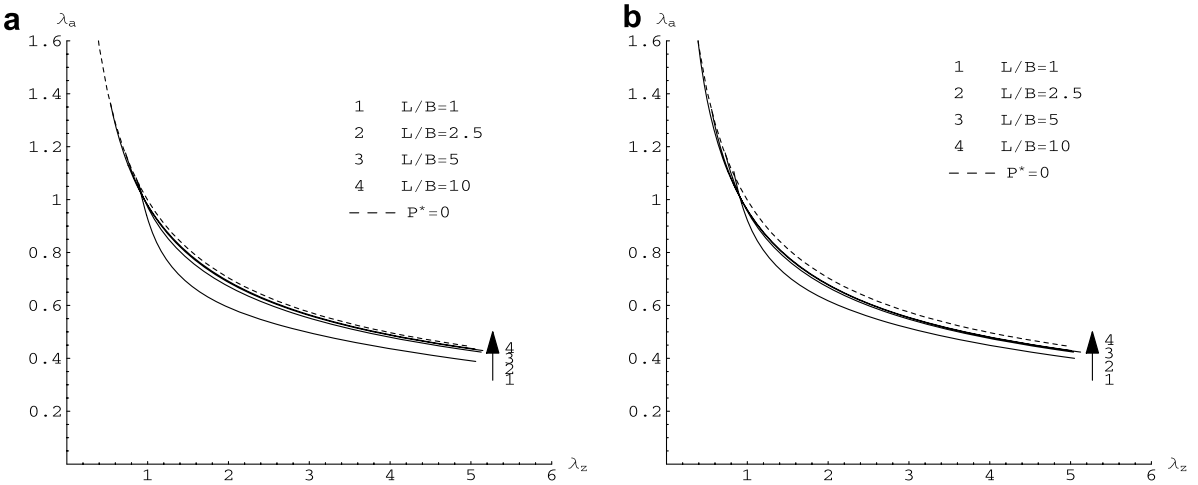

Fig. 6. As in Fig. 4 but for (a) $m = 3$ and (b) $m = 4$.

sure for higher mode numbers, while for longer tubes, mode 2 become the most unstable mode. The differences in these modes can be seen more clearly in Fig. 7. Note that compared with higher modes, the mode 1 curve is much further from the $P^* = 0$ curve, especially as axial extension is increased. This means that unless the tube is slightly compressed, a much greater pressure is required for a tube to buckle into mode 1 than into higher modes. This trend is even stronger for the longer tubes.

6.3.2. Thicker tube

To illustrate the influence of different mode numbers on the behaviour of thicker tubes, we plot the bifurcation curves for $m = 1, 2, 3, 4$ in Fig. 8 for $A/B = 0.5$ separately for each value $L/B = 1$ and $L/B = 5$. In Fig. 8(a), for $L/B = 1$, it can be seen that the bifurcation behaviour for the thicker tube is similar to that for the thinner tube, i.e. curves of modes 2, 3 and 4 are closer to each other than that for mode 1. Thus, under extension the tube may bifurcate into any of the modes 2, 3 and 4 but a relatively larger pressure is needed for mode 1 to be activated. Two major differences are observed between thinner and thicker tubes. One is that the mode 2, 3 and 4 curves are more separated for the thicker tube, the other is that for axial compression ($\lambda_z < 1$) the lower modes occur first, while for axial extension, mode 2 becomes the preferred mode for all values of λ_z.

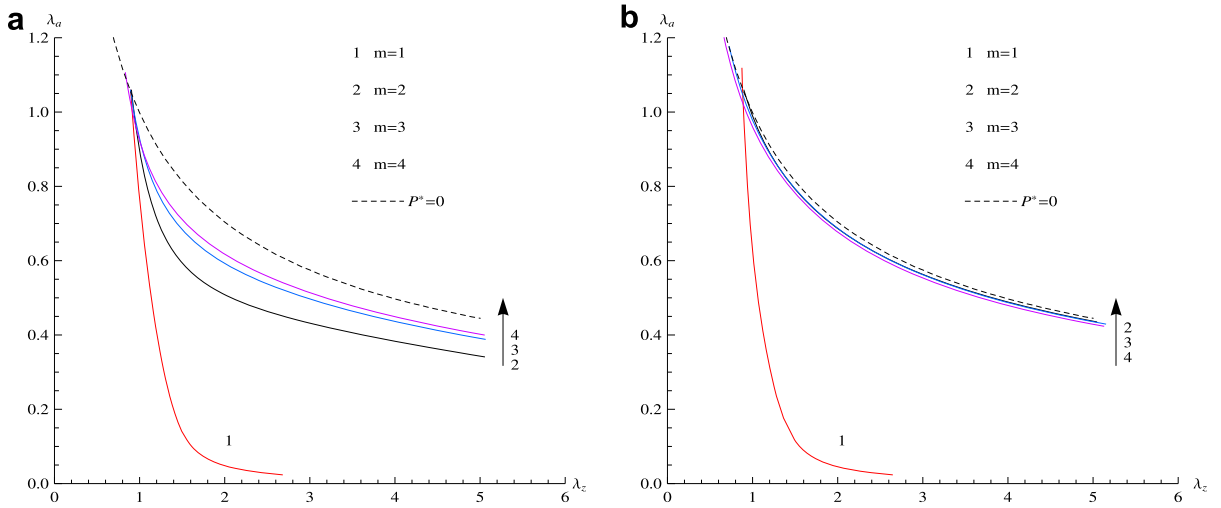

Fig. 7. Asymmetric bifurcation curves for $m = 1, 2, 3, 4$ and $A/B = 0.85$ in (λ_z, λ_a) space: (a) $L/B = 1$; (b) $L/B = 5$.

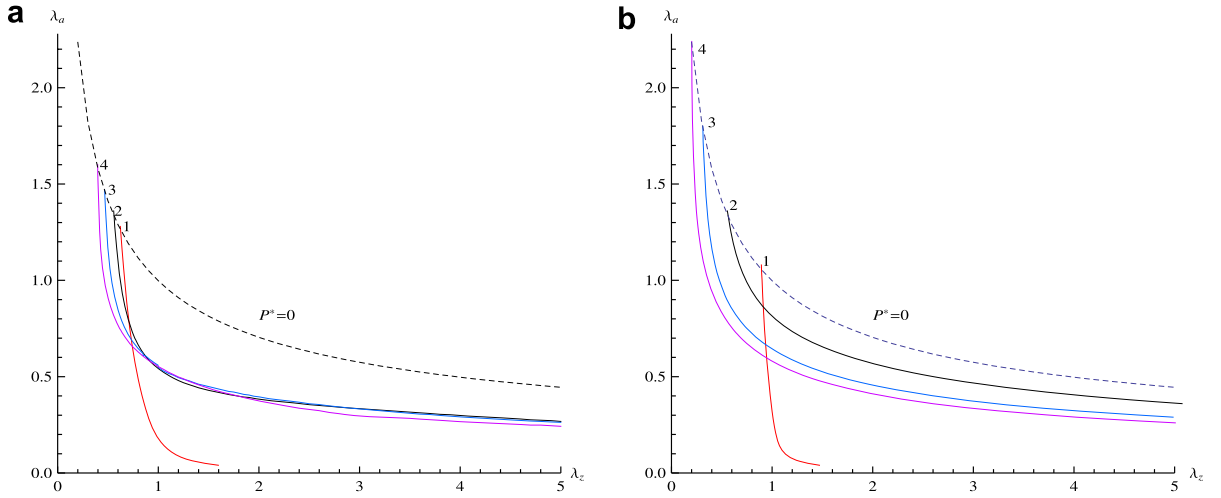

Fig. 8. Asymmetric bifurcation curves for $m = 1, 2, 3, 4$ and $A/B = 0.5$ in (λ_z, λ_a) space: (a) $L/B = 1$; (b) $L/B = 5$.

This is consistent with experimental observations and classical thin shell theory but is not so obvious for thinner tubes.

Fig. 8(b) shows corresponding results for $L/B = 5$. The curves for modes 2, 3 and 4 do not intersect. Compared with the $L/B = 1$ tube, the separations of the curves for $m = 2, 3, 4$ are relatively large. The mode 1 curve has one point of intersection with each of the other higher mode curves. In the region of axial extension, as the external pressure increases, bifurcation occurs first in mode 2, followed by modes 3, 4 and 1 successively. For modes 3 and 4, the bifurcation values of λ_a (larger than 1) along the equal pressure curve $P^* = 0$ for $L/B = 5$ are larger than those for $L/B = 1$.

6.3.3. Bifurcation pressure

Since mode 2 is the most widely observed mode in tube collapse experiments (Bertram, 1987), we show the mode 2 bifurcation pressure against L/B in Fig. 9 for both $A/B = 0.5$ and $A/B = 0.85$ for comparison, with $\lambda_z = 1$ in each case. It can be seen that the curves tend to flatten when $L/B \geqslant 4$. This suggests that, for longer tubes, wall thickness rather than tube length is more important in determining the magnitude of the bifurcation pressure. As a result, the value of the bifurcation pressure P^* for $A/B = 0.85$ is much smaller than that for

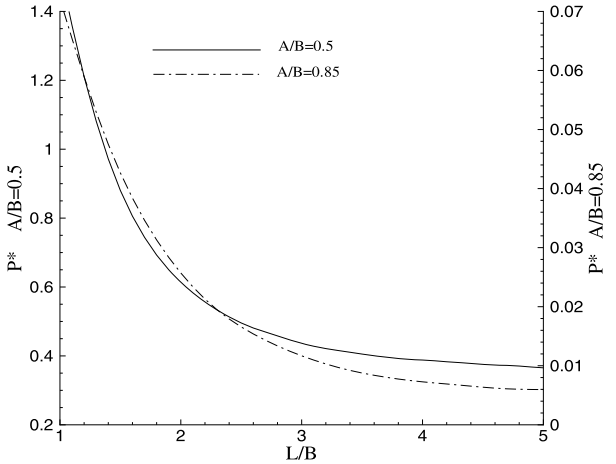

Fig. 9. Plot of $P^* = P/\mu$ at bifurcation (mode $m = 2$) against L/B for $A/B = 0.5$ (continuous curve, left-hand scale) and $A/B = 0.85$ (dash-dot curve, right-hand scale) and $\lambda_z = 1$.

$A/B = 0.5$, and this will be discussed further later in this section. It should be noted that different vertical scales are used for the two plots.

To see the change of the bifurcation pressure with wall thickness and to compare our results with those in the literature (Bertram, 1987; Marzo et al., 2005; Weissman and Mockros, 1967) we use the reference wall thickness $H = B - A$ and the parameters D, Q and P_k, defined by

$$D = \frac{2(B-A)}{\ln(B/A)}, \quad Q = \frac{EH^3}{12(1-\nu^2)}, \tag{67}$$

and

$$P_k = \frac{Q}{(D/2)^3} = \frac{2E}{3(1-\nu^2)}\left(\frac{H}{D}\right)^3, \tag{68}$$

where, in the context of classical elasticity, E is Young's modulus and ν is Poisson's ratio. Here, D denotes the logarithmic mean diameter and Q is the flexural rigidity of the tube wall. The pressure P is non-dimensionalized by dividing by P_k.

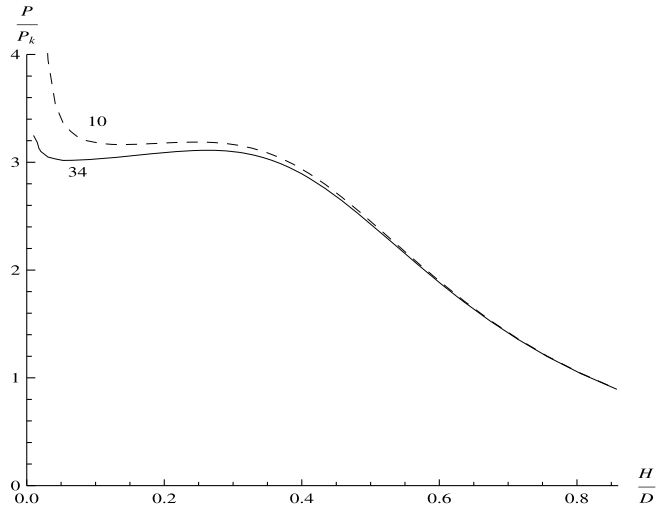

Fig. 10. Mode 2 bifurcation pressure plotted in dimensionless form as P/P_k against H/D for $L/B = 10$ (dashed curve) and $L/B = 34$ (continuous curve) and $\lambda_z = 1.005$.

Using the bifurcation criterion (60) combined with Eqs. (19), $(67)_1$ and (68), we obtain the mode 2 bifurcation pressure shown in Fig. 10, plotted with P/P_k against H/D. We see that the thinner tube begins to bifurcate at a pressure close to the theoretical value $P/P_k = 3$ in the thickness range of 0.05–0.4 in agreement with von Mises' prediction obtained from classical linear elasticity thin shell theory (von Mises, 1914). We emphasize again that our results are obtained from the incremental equations based on the full 3D theory of nonlinear elasticity, which provide the *exact* linearized bifurcation theory of elasticity, and our calculations are valid for underlying finite elastic deformations. To compare with Bertram's experimental results (Bertram, 1987) and the numerical results of Marzo et al. (2005), the parameter $L/B = 34$ was used here. In fact, our results indicate that, for tubes with $L/B = 10$ and $L/B = 34$, when $0.05 < H/D < 0.4$ the values of P/P_k are in the range 2.9–3.2. This explains why von Mises' prediction is confirmed by many different experiments and numerical simulations (Bertram, 1987; Marzo et al., 2005; Weissman and Mockros, 1967). In Bertram (1987) and Marzo et al. (2005), only some limited values of P/P_k were presented for a set of given values of H/D. Likewise, in Weissman and Mockros (1967), results were only presented for $0 < H/D < 0.25$. Here, the bifurcation pressure is shown for a much wider range of H/D. It is interesting to note that the bifurcation pressure does not change significantly for tubes with thickness ratio $0.05 < H/D < 0.4$.

However, our results show that towards the two ends of the H/D axis, the values of the bifurcation pressure for mode 2 differ from the classical prediction. For $H/D < 0.05$, the values of P/P_k are larger than 3. The shorter the tube, the greater the increase. For $L/B = 34$, $P/P_k = 3.24$ at $H/D = 0.01$ and for $L/B = 10$, it increases to 11.5 (see Fig. 10 and the $B/H = 50$ curve in Fig. 12). This discrepancy may be because in classical thin shell theory (Yamaki, 1984) the pre-buckling state was assumed to be a membrane stress state. When $H/D < 0.05$ and $L/B < 34$, neglect of the curvature of the deflected surface caused by external pressure can lead to serious error (von Mises, 1914). However, von Mises' formula $P_{\text{collapse}} = 3P_k$ is sufficiently accurate for shells with $L/B > 34$ (see page 73 in Yamaki (1984)). For $H/D > 0.4$, the curves for $L/B = 10$ and $L/B = 34$ almost coincide. The bifurcation pressure P/P_k drops below 3 as H/D increases, and decreases to 1 when $H/D = 0.8$. Caution is required with the physical interpretation of this result, since P_k is cubic H/D, which increases much faster than P as H/D is increased from 0.4. This trend can also be seen clearly in Fig. 13(a). In physical terms, a greater bifurcation pressure is still required to buckle the thicker tube, as expected, even though the ratio P/P_k is smaller.

6.3.4. Very short tubes

To illustrate further the dependence on tube length we now investigate briefly bifurcation of very short cylinders under axial compression and tension. Fig. 11(a) presents bifurcation curves in (λ_z, λ_a) space for tubes with $L/B = 0.5$ and $A/B = 0.5$. Transition from low to high mode occurs in the range of axial compression at an intersection point where $\lambda_z \approx 0.62$. When $\lambda_z < 0.62$, modes 1,2,3 occur first, while for $\lambda_z > 0.62$, the mode

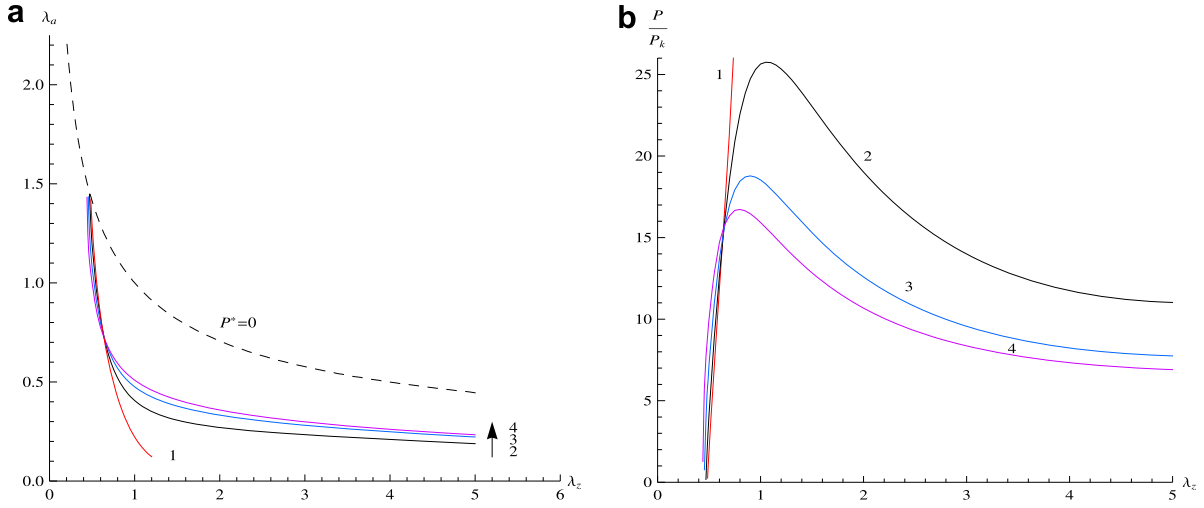

Fig. 11. Asymmetric bifurcation curves for $m = 1, 2, 3, 4$, $L/B = 0.5$ and $A/B = 0.5$. (a) In (λ_z, λ_a) space; (b) in $(\lambda_z, P/P_k)$ space.

$m = 4$ becomes the most unstable one. Referring back to Fig. 8(b) for $L/B = 5$ we see that, by contrast, there is no intersection point among curves for $m = 2, 3, 4$ and the mode 2 curve is above the others in the whole range of λ_z except in the short interval $0.90 < \lambda_z < 0.95$ where the mode 2 curve is below that for mode 1. Axial extension does not affect the order of the bifurcation modes for either of the tubes with $L/B = 1$ and $L/B = 5$. The parameter L/B therefore plays a major role in the transition from high to low modes, which is also found for tubes with $A/B = 0.85$. The results represented in Fig. 11(a) are converted into the plots of P/P_k against λ_z in Fig. 11(b) by use of (67) and (68). Fig. 11(b) shows that the P/P_k curve for mode 1 increases rapidly and monotonically, while for each mode 2, 3 and 4 there is a pressure maximum, occurring at $\lambda_z = 1.05, 0.90, 0.80$, respectively. Tubes subjected to sufficiently large axial compression or tension tend to bifurcate easily, while for $0.8 < \lambda_z < 1.05$ bifurcation requires a larger pressure. We can therefore conclude that either a large axial compression or axial tension reduces the axial stiffness of the cylinders.

6.3.5. The most unstable mode

To find the most unstable modes for different lengths and wall thicknesses, similarly to the predictions of classical thin shell theory (Yamaki, 1984), we plot the critical bifurcation curves in Fig. 12. It is seen that for a thin shell, $B/H = 50$, the results are in excellent quantitative agreement with those of Yamaki (1984) (Fig. 2.12, for boundary condition S4). There exists only a small discrepancy due to the slightly different boundary conditions used here. In other words, if the wall is thin, then higher modes are more unstable for shorter tubes. However, as the wall thickness is increased, the critical higher modes become fewer, and mode 2 becomes more and more dominant. Eventually, for $B/H < 2$ and $L/B > 1.2$ it remains the only bifurcation mode. For instance, in the range of $4 < L/B < 10$, a thin tube with $B/H = 50$, bifurcates into the $m = 2$ mode, whereas thick-walled tube with $B/H = 6.67$, bifurcates into the $m = 3$ mode. In the context of axial compression of steel cylinders undergoing plastic deformation a very similar distribution of bifurcation modes was found by Bardi and Kyriakides (2006) experimentally and (Bardi et al., 2006) analytically. Apart from the type of material behaviour, this differs from the present analysis since we are considering external pressure rather than axial compression and we have fixed $\lambda_z = 1$ in Fig. 12. Fig. 7(a) shows that for tubes with $A/B = 0.85$ (equivalent to $B/H = 6.67$) under external pressure and axial extension, the higher modes are more unstable. Another interesting phenomenon is that the thicker the tube the smaller the value of L/B at which the curve flattens. The curves for tubes with $B/H = 50, 6.67, 2$ show that as $L/B \to \infty$, P/P_k approaches 3.0, which is in agreement with the thin shell theory prediction. But for the very thick tube with $B/H = 1.58$, P/P_k approaches 2.43. The bifurcation pressure for thick tubes with $H/D > 0.4$ drops below 3.0 (see also Fig. 10).

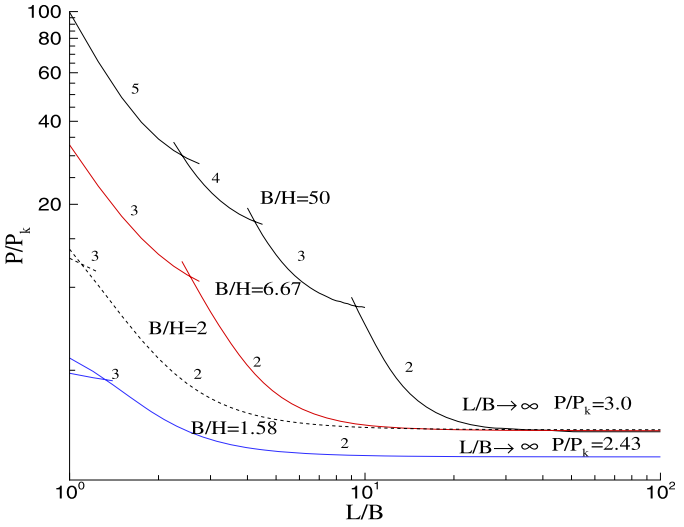

Fig. 12. Bifurcation pressure plotted in dimensionless form as P/P_k against L/B for $B/H = 50$ (black curves), $B/H = 6.67$ (red curves), $B/H = 2$ (dashed curves), $B/H = 1.58$ (blue curves) with different mode numbers and $\lambda_z = 1$. (For interpretation of the references to color in this figure legend, the reader is referred to the web version of this article.)

6.4. Discussion

In this paper, we have investigated the non-linear buckling behaviour of thick-walled circular cylinder tubes under external pressure combined with axial loading. Our study is particularly useful in determining the buckling of thick-walled tubes, which is beyond the limit of validity of thin shell theory. This work has been conducted with a background in mind of the bifurcation behaviour of collapsible tubes conveying internal flow, although we note that the essential difference between this study and studies by the collapsible tube flow community (Heil, 1996; Heil and Pedley, 1996; Bertram et al., 1990) is that no fluid–structure interactions are considered. Here, the (external) pressure is acting as a (prescribed) static load, which contrasts with the strong viscous pressure when an internal flow is present. However, in the context of critical buckling, it has been found that these different mechanisms (static pressure load or flow-induced pressure load) lead to similar results except that a substantially higher pressure drop is required to achieve the same level of collapse for the static load case (Heil and Pedley, 1996).

The most interesting finding is that for wall thickness ratios A/B greater than about 0.5, mode 2 seems to be the dominant critical buckling mode unless the tubes are extremely short (e.g., $L/B \lesssim 1.2$). This is different from the predictions of classical thin shell theory (Yamaki, 1984), but agrees with the fact that in many thick-walled tube experiments, in particular those of Bertram (1982, 1987) and Bertram et al. (1990), only mode 2 buckling has been observed regardless of the tube length used. The fact that in experiments the prevailing mode is mode 2 cannot be fully explained by thin shell theory. This is because when fluid–structure interaction is involved, the effect of the fluid flow is to increase the viscous pressure drop, which induces an additional compressive load at the downstream end of the tube. As a result, only the compressed downstream part of the tube actually participates in the buckling, which is then similar to the buckling of a short tube (Heil and Pedley, 1996). If the thin shell theory were to be valid, this would induce the buckling to occur in a higher mode. The reason why this did not happen in the experiments is that, for thicker tubes, mode changes no longer happen, and long thick tubes were used in experiments (Bertram, 1987; Bertram et al., 1990). As illustrated in Fig. 12, for long thick tubes, only mode 2 occurs. As indicated above, our study shows that if A/B is greater than about 0.5, then the critical buckling mode will remain as mode 2 except for very short tubes.

Although the von Mises formula is derived for thin-walled tubes, experimental measurements have shown that it also predicts the bifurcation pressure for thick-walled tubes reasonably well (Weissman and Mockros, 1967). Our results show that this is because the bifurcation pressure P/P_k is insensitive to the change of wall thickness H/D for the range of $0.05 < H/D < 0.4$. If the tube is sufficiently thin or sufficiently thick, then the von Mises formula is no longer accurate, and P/P_k actually increases in the thin wall extreme, and decreases in the thicker wall region.

In order to have a more direct comparison with the Weissman and Mockros experiments, we plot the bifurcation pressure in terms of P against H/D in Fig. 13. This is obtained using the bifurcation criterion (60) combined with Eq. (19) and the equation

$$\mu = \frac{E}{2(1+\nu)}, \tag{69}$$

where (for an incompressible material) $\nu = 0.5$. The value $E = 300\,\text{psi}$ ($= 2.07\,\text{MPa}$) adopted by Weissman and Mockros then gives $\mu = 0.69\,\text{MPa}$, which is used to calculate the bifurcation pressure.

It can be seen that for a very thin tube ($0 < H/D < 0.1$), bifurcation occurs at a small external pressure. For tubes with larger wall thickness, when $H/D > 0.1$, the bifurcation pressure increases rapidly. For $0 < H/D < 0.4$, our results are in accord with the experimental results of Weissman and Mockros (1967) and von Mises' formula. When $H/D > 0.4$, the latter curve increases more rapidly than for our results.

Although we have considered a tube of finite length, a limitation of the present study is that we have initiated the bifurcation analysis from a deformed circular cylindrical configuration and adopted rather special incremental boundary conditions on the ends of the tube. These might prevent realistic post-buckling behaviour for which large deformations can occur in either the axial or azimuthal direction near the ends. Thus, our results only apply for the initial bifurcation behaviour. Many interesting phenomena, such as self-exited oscillations in collapsible tubes conveying fluid, occur in the post-buckling phase, where the cross-sectional area typically takes on an elliptical or dumbbell shape. These are excluded in the present analysis.

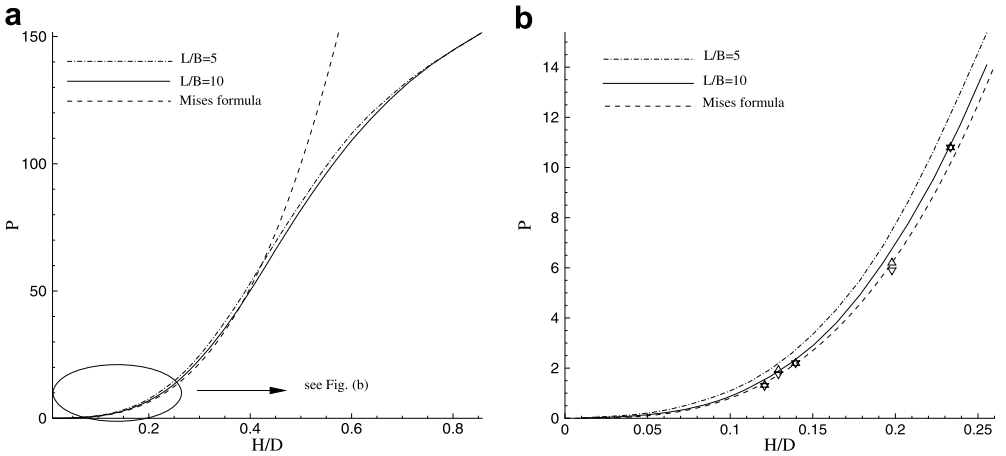

Fig. 13. (a) Mode $m = 2$ bifurcation pressures P vs. H/D for silicone rubber tubes for $\lambda_z = 1.005$; the continuous curve is for $L/B = 10$, and dash-dot curve is for $L/B = 5$. The dashed curve corresponds to von Mises' theoretical result. (b) the enlarged area indicated in (a). The symbols are from the Weissman and Mockros experimental results: ∇ represents bifurcation points at 50% volume collapse and $\triangle$ at 70%.

7. Conclusion

Axisymmetric and asymmetric bifurcations of circular cylinders under external pressure combined with axial loading have been analyzed in detail using a particular model strain-energy function appropriate for non-linear elastic deformations of rubberlike materials. Unlike the models used by von Mises (1914) and Yamaki (1984), which are applicable only for thin-walled tubes, this study presents results for a wide range of tube wall thickness on the basis of the exact 3D theory of finite elasticity. A more general description of the bifurcation behaviour of thick-walled tubes subject to external pressure combined with axial loading, including axial compression and extension, has been presented. Good agreement with previous studies has been found, and extensive comparisons with results for thin-shell theory are made. Our results show that the critical bifurcation pressure deviates from the thin shell prediction in both the very thin and thick-walled regimes. For very short and sufficiently thick tubes, transition from lower to higher modes occurs in the range of axial compression. We have also shown that, contrary to thin-shell theory, for sufficiently thick tubes, transition from lower to higher modes does not occur for sufficiently short tubes. Instead, mode 2 bifurcation becomes the sole dominant mode.

In the next phase of this work we shall investigate the post-buckling behaviour of elastic tubes under external pressure and axial loading. In particular, the effect of wall thickness on compliance of the tubes between buckling and self-contact will be studied in order to interpret the puzzling phenomenon that for tubes subjected to external pressure, after a certain degree of collapse, thick tubes may be more compliant than thinner ones (Bertram, 1987; Marzo et al., 2005).

Acknowledgements

The authors are grateful to Dr. David Haughton, University of Glasgow, and Professor Chris Bertram, University of New South Wales, for their valuable advice.

References

Amabili, M., Païdoussis, M.P., 2003. Review of studies on geometrically nonlinear vibrations and dynamics of circular cylindrical shells and panels, with and without fluid–structure intersection. Applied Mechanics Reviews 56, 349–381.

Bardi, F.C., Kyriakides, S., 2006. Plastic buckling of circular tubes under axial compression – Part I: Experiments. International Journal of Mechanical Sciences 48, 830–841.

Bardi, F.C., Kyriakides, S., Yun, H.D., 2006. Plastic buckling of circular tubes under axial compression – Part II: Analysis. International Journal of Mechanical Sciences 48, 842–854.

Batdorf, S.B., 1947. A simplified method of elastic stability analysis for thin cylindrical shells. NACA Report 874.
Bertram, C.D., 1982. Two modes of instability in a thick-walled collapsible tube conveying a flow. Journal of Biomechanics 15, 223–224.
Bertram, C.D., 1987. The effects of wall thickness, axial strain and end proximity on the pressure-area relation of collapsible tubes. Journal of Biomechanics 20, 863–876.
Bertram, C.D., Raymond, C.J., Pedley, T.J., 1990. Mapping of instabilities for flow through collapsed tubes of differing length. Journal of Fluids and Structures 4, 125–153.
Bertram, C.D., 1995. The dynamics of collapsible tubes. In: Ellington, C.P., Pedley, T.J. (Eds.), Biological Fluid Dynamics. The Company of Biologists Limited, Cambridge, UK, pp. 253–264.
Bertram, C.D., Elliot, N.S.J., 2003. Flow-rate limitation in a uniform thin-walled collapsible tube, with comparison to a uniform thick-walled tube and a tube of tapering thickness. Journal of Fluids and Structures 17, 541–559.
Flaherty, J.E., Keller, J.B., Rubinow, S.I., 1972. Post buckling behavior of elastic tubes and rings with opposite sides in contact. SIAM Journal of Applied Mathematics 23, 446–455.
Flügge, W., 1973. Stresses in Shells, Second ed. Springer, Berlin.
Gerald, C.F., Wheatley, P.O., 1984. Applied Numerical Analysis. Addison Wesley, New York.
Green, A.E., Rivilin, R.S., Shield, R.T., 1952. General theory of small elastic deformations superposed on finite elastic deformations. Proceedings of the Royal Society of London A 211, 128–154.
Haughton, D.M., Ogden, R.W., 1978a. On the incremental equations in non-linear elasticity – I. Membrane theory. Journal of the Mechanics and Physics of Solids 26, 93–110.
Haughton, D.M., Ogden, R.W., 1978b. On the incremental equations in non-linear elasticity – II. Bifurcation of pressured spherical shells. Journal of the Mechanics and Physics of Solids 26, 111–138.
Haughton, D.M., Ogden, R.W., 1979a. Bifurcation of inflated circular cylinders of elastic material under axial loading – I. Membrane theory for thin-walled tubes. Journal of the Mechanics and Physics of Solids 27, 179–212.
Haughton, D.M., Ogden, R.W., 1979b. Bifurcation of inflated circular cylinders of elastic material under axial loading – II. Exact theory for thick-walled tubes. Journal of the Mechanics and Physics of Solids 27, 489–512.
Heil, M., 1996. The stability of cylindrical shells conveying viscous flow. Journal of Fluids and Structures 10, 173–196.
Heil, M., Pedley, T.J., 1996. Large post-buckling deformations of cylindrical shells conveying viscous flow. Journal of Fluids and Structures 10, 565–599.
Ho, B.P.C., Cheng, S., 1963. Some problems in stability of heterogeneous aeolotropic cylindrical shells under combined loading. AIAA Journal 1, 1603–1607.
Kounadis, A.N., 2006. Recent advances on postbuckling analyses of thin-walled structures: beams, frames and cylindrical shells. Journal of Constructional Steel Research 62, 1101–1115.
Luo, X.Y., Pedley, T.J., 1996. A numerical simulation of unsteady flow in a 2D collapsible channel. Journal of Fluid Mechanics 314, 191–225.
Luo, X.Y., Pedley, T.J., 1998. The effects of the wall inertia on the 2D collapsible channel flow. Journal of Fluid Mechanics 363, 253–280.
Luo, X.Y., Pedley, T.J., 2000. Flow limitation and multiple solutions in 2D collapsible channel flow. Journal of Fluid Mechanics 420, 301–324.
Luo, X.Y., Cai, Z.X., Li, W.G., Pedley, T.J., 2008. The cascade structure of linear stabilities of flow in collapsible channels. Journal of Fluid Mechanics 600, 45–76.
Marzo, A., Luo, X.Y., Bertram, C.D., 2005. Three-dimensional collapse and steady flow in thick-walled flexible tubes. Journal of Fluids and Structures 20, 817–835.
Nash, W.A., 1954. Buckling of thin cylindrical shells subject to hydrostatic pressure. Journal of the Aeronautical Sciences 21, 354–355.
Nowinski, J.L., Shahinpoor, M., 1969. Stability of an elastic circular tube of arbitrary wall thickness subjected to an external pressure. International Journal of Non-linear Mechanics 4, 143–158.
Ogden, R.W., 1972. Large deformation isotropic elasticity – on the correlation of theory and experiment for incompressible rubberlike solids. Proceedings of the Royal Society of London A 326, 565–584.
Ogden, R.W., 1974. On stress rates in solid mechanics with application to elasticity theory. Proceedings of the Cambridge Philosophical Society 75, 303–319.
Ogden, R.W., 1997. Non-linear Elastic Deformations. Dover Publications, New York.
Sobel, L.H., 1964. Effects of boundary conditions on the stability of cylinders subject to lateral and axial pressure. AIAA Journal 2, 1437–1440.
von Mises, R., 1914. Der kritische Außendruck zylindrischer Rohre. VDI Zeitschrift 58, 750–755.
Wang, A.S.D., Ertepinar, A., 1972. Stability and vibrations of elastic thick-walled cylindrical and spherical shells subjected to pressure. International Journal of Non-linear Mechanics 7, 539–555.
Weissman, M., Mockros, L., 1967. The mechanics of a collapsing tube heart pump. International Journal of Mechanical Sciences 9, 113–121.
Yamaki, N., 1969. Buckling of circular cylindrical shells under external pressure. Reports of the Institute of High Speed Mechanics 20, 35–55.
Yamaki, N., 1970. Influence of prebuckling deformation on the buckling of circular cylindrical shells under external pressure. Reports of the Institute of High Speed Mechanics 21, 81–104.
Yamaki, N., 1984. Elastic Stability of Circular Cylindrical Shells. North-Holland, Amsterdam.